

NONDESTRUCTIVE CHARACTERIZATION OF THE ELASTIC CONSTANTS
 OF FIBER REINFORCED COMPOSITES

Ajit K. Mal and Shyh-Shiuh Lih
 Mechanical, Aerospace and Nuclear Engineering Department
 University of California Los Angeles, California

Yoseph Bar-Cohen
 Jet Propulsion Laboratory
 Pasadena, California

Abstract

Composite structural components may be subjected to a variety of defects resulting in a sharp reduction in their load carrying capacity or even catastrophic failure. Thus, it is extremely important to have the means to monitor the degradation suffered by critical components of a structure for safe operation during its service life. A nondestructive method based on ultrasonics has recently been developed for the quantitative evaluation of composite structural components during service. The experimental part of the technique uses a two-transducer, pitch-catch type arrangement to generate a variety of elastic waves within the specimen immersed in water. The recorded reflection data are then analyzed by means of a theoretical model to back out the relevant properties. In this paper the method is applied to determine the stiffness constants of unidirectional graphite/epoxy materials. The measurements are shown to be efficient and sufficiently accurate so that it can be used for early detection of material degradation in composite structural elements during service.

Nomenclature

$v, V_1, V_2, v,$	wave speeds
θ	incident angle
ϕ	fiber orientation
ϕ_c	critical angle
σ_{ij}	Cauchy's stress tensor
C_{ij}	elastic constants
ρ	density
u_i, U_i	displacement
a_1, a_2, \dots, a_3	defined in eq. (4)
ξ_i	slowness on the x_1 - x_2 plane
k_i	wave numbers
ζ_i	slowness along x_3
$b_i, \alpha, \beta, \gamma$	parameters defined in eq. (7)
t_{kl}	arrival time of wave mode kl
H	laminate thickness

I. Introduction

All aircraft and aerospace structural components and their mechanical subcomponents are subjected to service conditions that lead to a deterioration of their performance and integrity with time. This is primarily due to the fact that structural materials suffer degradation as they age¹ resulting in changes in their properties and reducing their load carrying capacity. In absence of timely diagnosis of the degree of deterioration and appropriate intervention, the structure in question may suffer catastrophic failure. Factors that cause materials degradation include extensive cyclic loading (mechanical and thermal); exposure to extreme temperatures; excessive humidity, chemical attack, foreign object impact, rapidly applied thermal loading etc.

Composite materials are being used increasingly in many structures and their subcomponents. Fiber reinforced composites, e.g., graphite/epoxy are the most widely used materials in aircraft structures at the present time. These materials provide a very desirable combination of toughness, specific strength, modulus and damage tolerance. However, composites are very sensitive to their manufacturing processes, service conditions and the natural environment, either one or all of which may introduce defects resulting in a serious degradation of the material. Further, as these materials age, they will be subject to a variety of degradations and the need for their evaluation and repair/rejection will become more and more critical.

A major factor in the expanded use of composites at low operating costs is adequate nondestructive evaluation (NDE) technology. Development of sound science-based techniques to detect hidden, subsurface damage and material degradation prior to structural failure is of critical importance for the design and deployment of aircraft and aerospace structures of the future. A number of NDE techniques are available for the inspection of structural components. Some of

the . . . e.g., X-Ray and Gamma Ray radiography are of relatively low sensitivity and are not suitable for the characterization of material degradation. A more sensitive radiographic technique, the neutron radiography, is expensive, nonportable and is affected by the presence of hydrogen compounds (e.g., trapped moisture and sealing materials) in the damaged area. Electromagnetic methods (e.g., eddy current probes) work reasonably well for metals but are unsuitable for nonmetallic composites. The most cost effective and generally applicable NDE methods are based on ultrasonics. The conventional pulse – echo and through – transmission methods are simple to implement, but they provide only limited information in the interior of the structure.

Several recently developed ultrasonic techniques appear to have the potential for improving the state – of – the – art in NDE technology significantly through additional research. One of these is the “leaky Lamb wave (LLW)” technique in which the specimen is immersed in water and tested by two broadband ultrasonic transducers in a pitch – catch arrangement. In this method a variety of waves are generated within the specimen and each of these waves carries specific information on the characteristics of the material. Careful analysis of the recorded waveforms can, in principle, unravel this information.²⁻⁴

In this paper we apply the LLW technique to determine the stiffness constants of unidirectional graphite epoxy materials. A systematic procedure proposed by Karim, Mal and Bar-Cohen⁵ by inverting the LLW dispersion data has been found to be an effective method to characterize the elastic constants of graphite epoxy composites. We give a brief description of this method, and through a carefully conducted parameter study, show that only the matrix dominated stiffness constants c_{22} , c_{23} and c_{33} can be determined accurately by this method. The fiber dominated constants, c_{11} and c_{12} can not be determined accurately by this procedure due to the fact that the Lamb wave velocity is insensitive to c_{11} and c_{12} in the range in which the dispersion data are reliable.

In this paper we describe a new technique which can be used to determine all five stiffness constants by analyzing the times of flight of the recorded reflected acoustic waves in a pulsed LLW experiment. A generalized ray theory described in Malet al⁶, is used to identify the modality and ray path of each arrival; the time of flight of each ray is then related to the

elastic constants of the composite. The accuracy of the inversion procedure is discussed.

11. The Ultrasonic Experiment

As indicated in the preceding section, the ultrasonic experiment is based on an oblique insonification of the specimen immersed in water. The acoustic wave is transmitted from a broadband transducer and the reflected signal is recorded by a second transducer in a pitch-catch arrangement as shown in Fig. 1.

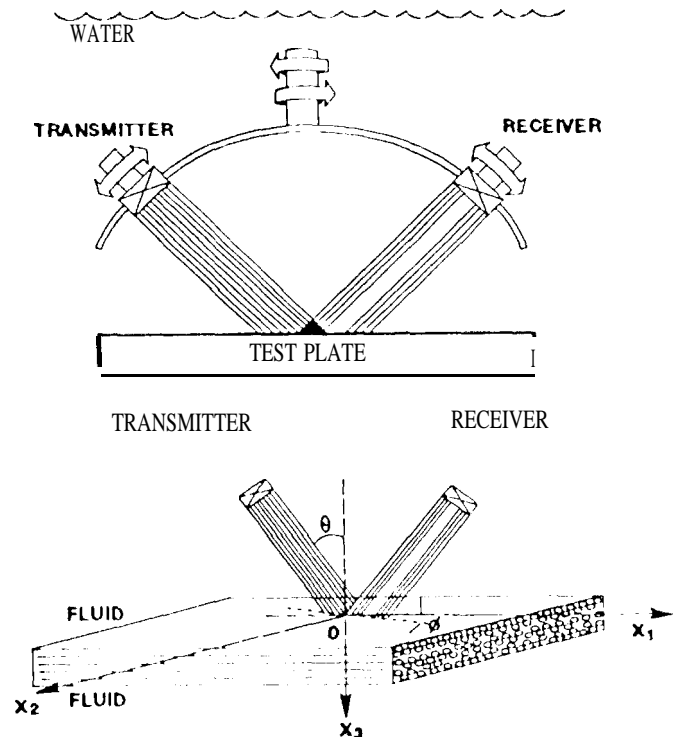


Fig. 1. The experimental setup.

A number of flat, broadband transducers with center frequencies in the range of 0.5 - 10 MHz are used and the signals, transmitted either in tone-burst or short pulse form are used to study the material characteristics. The tone-burst signals are generated by a function generator to establish a steady-state condition. At a specific angle of incidence the

reflected signal is recorded as a function of frequency, amplified, averaged and digitized with the aid of a box-car gated integrator. The amplitude spectrum of the recorded reflected signal is obtained by changing the frequency of the continuous wave signal. If the angle of incident, θ , of the acoustic waves is greater than certain critical value, multi-modal dispersive guided waves are induced in the specimen at a finite number of specific frequencies of excitation. The guided waves propagate in a direction parallel to the surface-s of the specimen and leak energy into the surrounding fluid. The leaky wave-s combine with the specularly reflected waves to form minima or "nulls" in the amplitude spectra of the reflected signal at the modal frequencies of the guided waves. The phase velocity, V , of the guided waves is related to the angle of incidence, θ , through Snell's law:

$$V = \alpha_0 / \sin \theta$$

where α_0 is the acoustic wave speed in the fluid. Thus, for a given angle of incidence, the minima or nulls in the reflection amplitude spectrum are associated with the excitation of leaky guided waves in the specimen.

The dispersion curves for the specimen can be determined from the amplitude spectra of the reflected waves recorded as functions of the incident angle. The material constants and the thickness of the specimen are related to the dispersion curves and can be determined by fitting the experimental curves with those obtained from theory.

In the second method proposed here, pulsed signals are transmitted in either a pulse-echo or pitch-catch arrangement.³ The reflected signals in the time domain are recorded and if there is clear separation between the individual pulses, their measured times-of-flight are used to determine the material constants through analysis.

III. Characterization of Material constants from Leaky Lamb Wave Experiment

As indicated in the introduction, this technique has been described in an earlier paper.⁵ The basic idea behind the technique is to obtain the experimental dispersion curves of leaky guided waves in the specimen from the ultrasonic test. These dispersion curves can also be obtained from theoretical models using nominal values of the five stiffness constants of the specimen. The stiffness constants are then

determined consistent with the "best fit" between the theoretical and measured curves. Fig. 2 is a comparison of between the measured and calculated dispersion curves for waves propagating at 0°, 45° and 90° to the fibers in a unidirectional graphite/epoxy laminate of 1 mm thickness. The material constants determined from inversion and used in the calculation are

$$\begin{aligned} c_{11} &= 160.73, & c_{12} &= 6.44, & c_{22} &= 13.92, \\ c_{23} &= 6.92, & c_{33} &= 7.07 \end{aligned}$$

where the units are in GPa.

It can be seen that a very good fit between the measured and calculated dispersion curves has been achieved. However, the relation between the calculated wave speed and the unknown stiffness constants is highly nonlinear and the solution to the inversion problem is nonunique. In addition, each stiffness constant has a different influence on the dispersion curves, and this can affect the accuracy of its estimated value. Data errors also play an important role in the inversion algorithm. These issues have not been carefully studied so far.

We have carried out a detailed and systematic parameter study of the influence of the five stiffness constants on the dispersion curves. Typical results of the study are presented in Figs. 3 and 4, for symmetric and antisymmetric Lamb waves propagating at 45° to the fibers; results for other propagation directions are similar. It can be seen that c_{22}, c_{23}, c_{33} have a strong influence on the dispersion curves. In addition, the first symmetric mode at the higher velocity range is strongly affected by c_{11} . The constant c_{12} does not seem to have significant influence on any of the branches. Thus it appears that the four constants $c_{11}, c_{22}, c_{23},$ and c_{33} can be determined accurately from the dispersion curves. However, at the high velocity range the incident angle is small ($\approx 10^\circ$), the set up is difficult and time consuming, and the errors in locating the minima in the dispersion curves are large. Thus, the procedure cannot be used to determine the constants, c_{11} and c_{12} accurately. In the next section we describe an alternative technique that is capable of giving accurate estimates of all five constants and, at the same time, is simpler to implement both in the laboratory and in field environments.

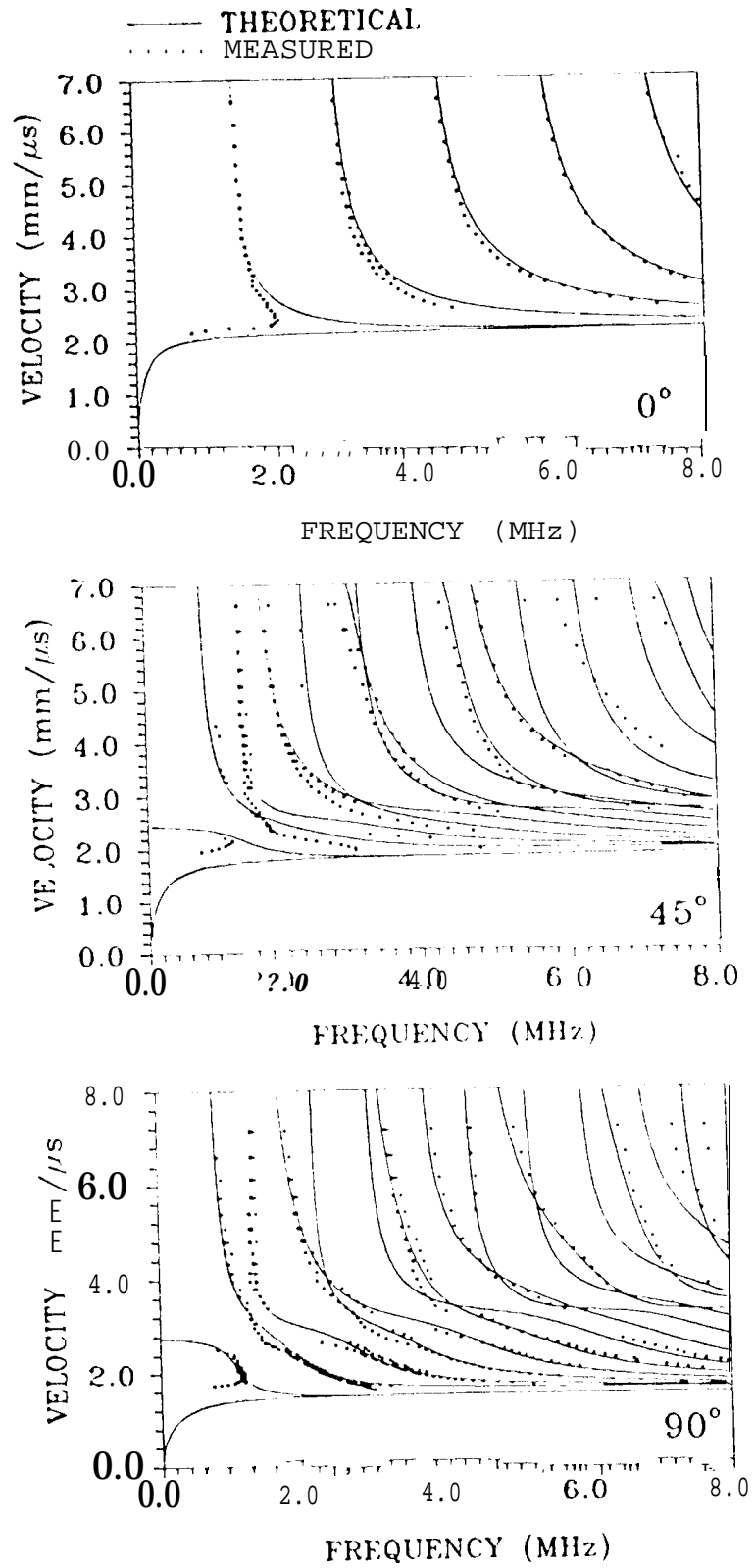


Fig. 2. Comparison between **measured** and calculated dispersion curves for a 1 mm thick graphite/epoxy laminate for waves propagating at 0°, 45° and 90° to the fibers.

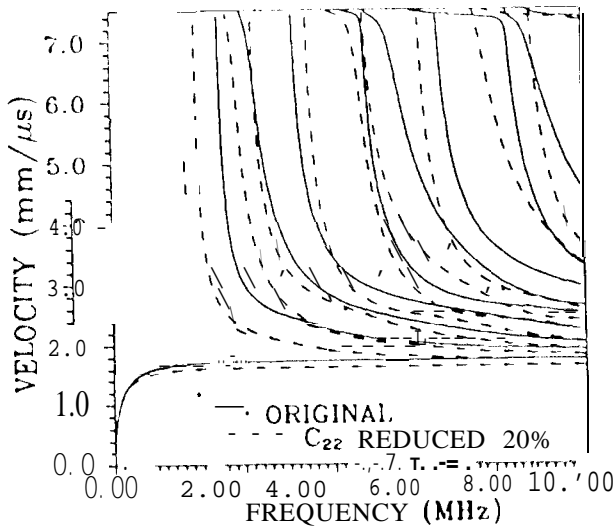
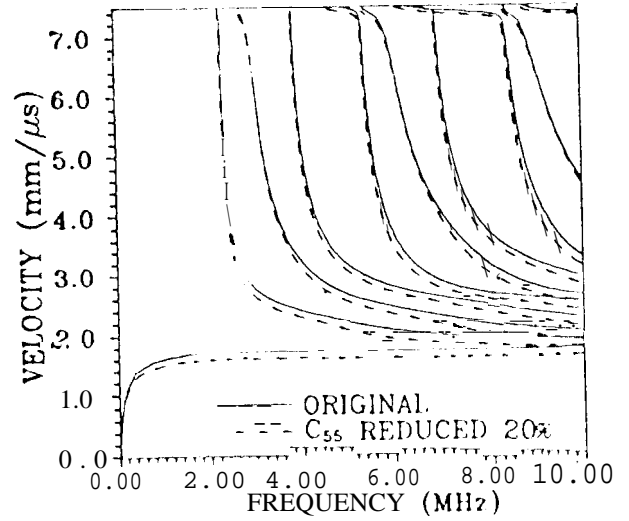
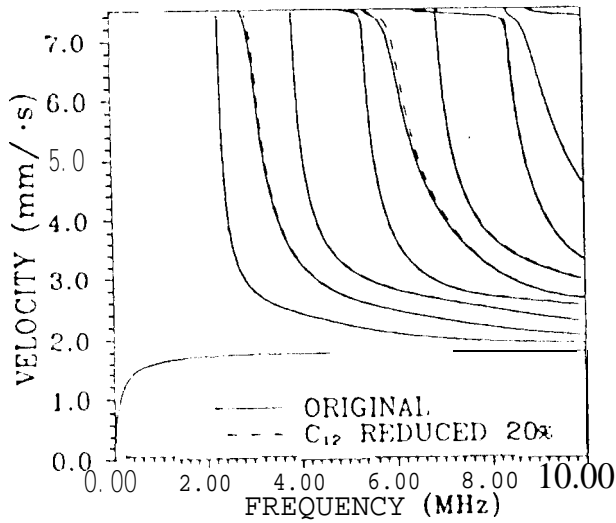
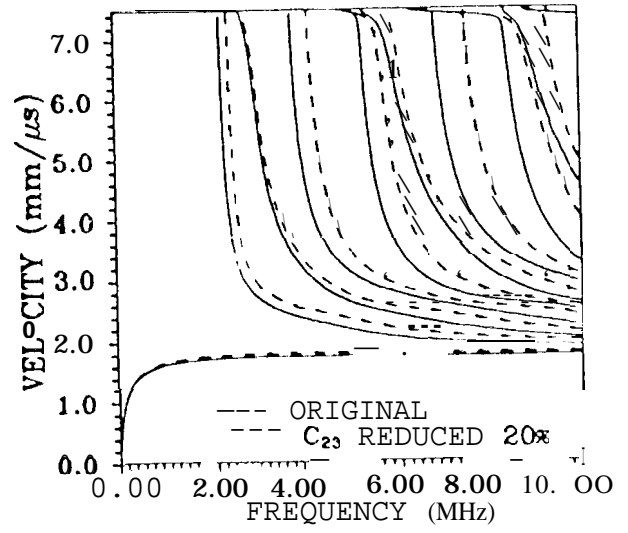
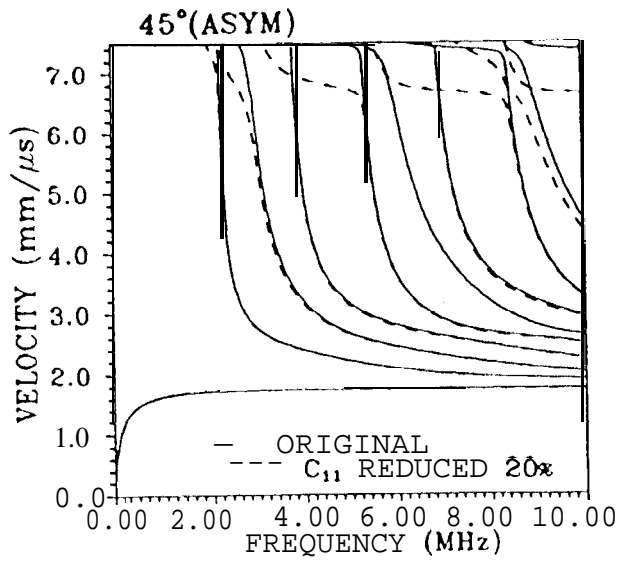


Fig. 3. Influence of the stiffness constants c_i on the dispersion curves for antisymmetric mode waves propagating at 45° to the fibers.

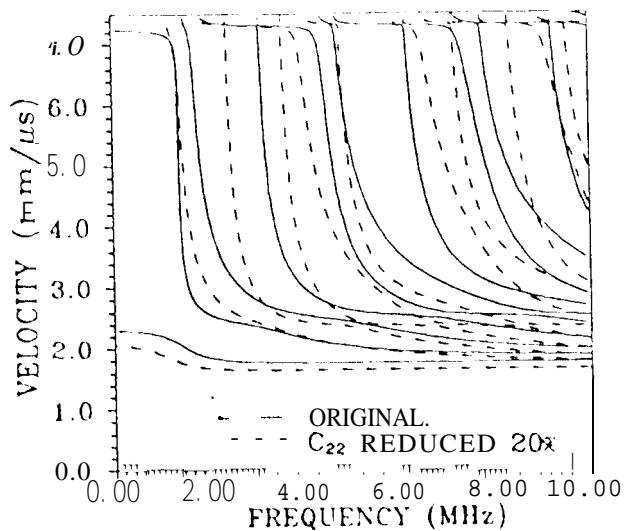
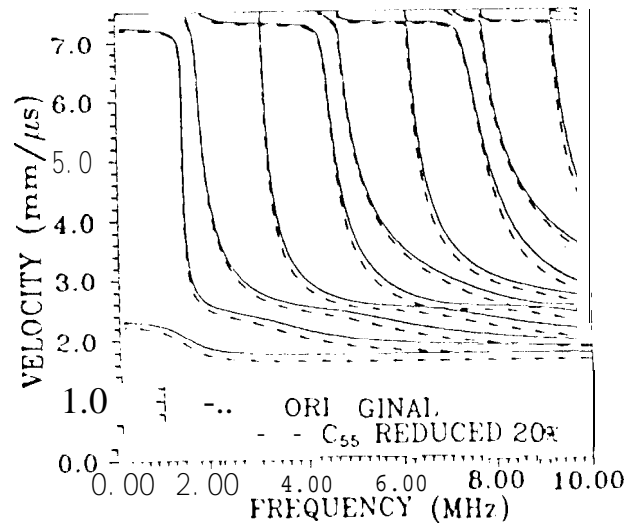
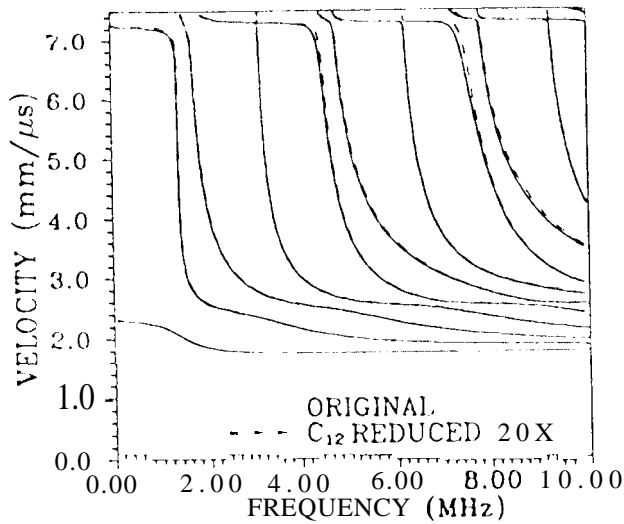
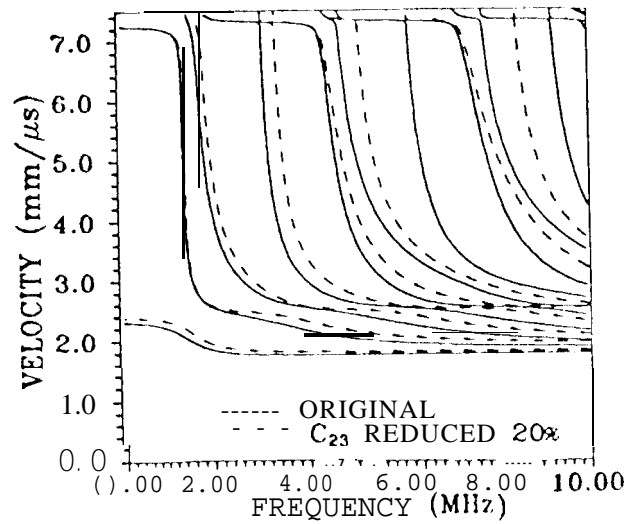
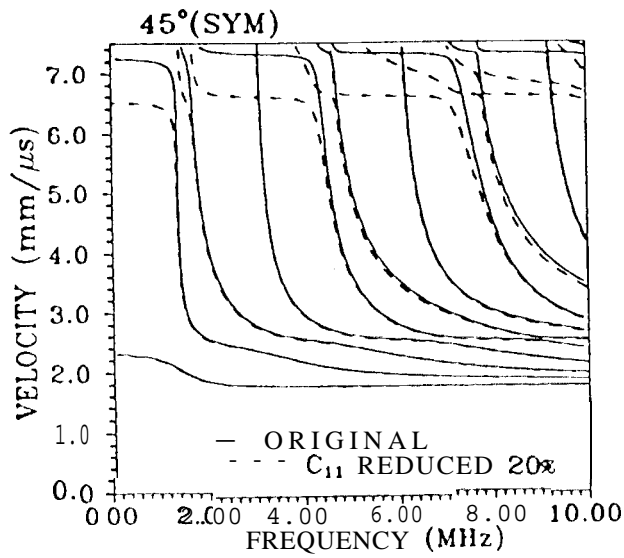


Fig. 4. Influence of the stiffness constants c_{ij} on the dispersion curves for symmetric mode waves propagating at 45° to the fibers.

IV. Characterization of the material constants from travel times of the reflected rays

Ray theory

Consider a unidirectional composite plate with thickness H and density ρ immersed in a fluid as shown in Fig. 1. Assume that the material is homogeneous and transversely isotropic with symmetry axis along x_1 and characterized by five stiffness constants, c_{11} , c_{12} , c_{22} , c_{23} , and c_{33} . The Cauchy's equation of motion for the material is

$$\sigma_{ij} - \rho \ddot{u}_i = 0 \quad (1)$$

where u_i is the displacement vector and σ_{ij} is the stress tensor. Assume plane wave solutions of (1) in the form

$$U_i = U_j e^{i(k_1 x_1 + k_2 x_2 + k_3 x_3) - i\omega t} \quad (2)$$

where k_1 , k_2 and k_3 represent the wavenumbers along the x_1 , x_2 and x_3 directions, respectively, and ω is the circular frequency. From (1), (2) and the constitutive relations for the material we obtain the following eigenvalue problem for calculation of the wave speed in a given direction:

$$\begin{bmatrix} a_2 \xi_1^2 + a_3 (\xi_2^2 + \zeta^2) - 1 & a_3 \xi_1 \xi_2 & a_3 \xi_1 \zeta \\ a_3 \xi_1 \xi_2 & a_3 \xi_1^2 + a_1 \xi_2^2 + a_2 \zeta^2 - 1 & (a_1 - a_2) \xi_2 \zeta \\ a_3 \xi_1 \zeta & (a_1 - a_2) \xi_2 \zeta & a_3 \xi_1^2 + a_2 \xi_2^2 + a_1 \zeta^2 \end{bmatrix} \begin{bmatrix} U_1 \\ U_2 \\ U_3 \end{bmatrix} = \begin{bmatrix} 0 \\ 0 \\ 0 \end{bmatrix} \quad (3)$$

where

$$\begin{aligned} a_1 &= c_{22}/\rho, \quad a_2 = c_{11}/\rho, \quad a_3 = (c_{12} + c_{33})/\rho \\ a_4 &= (c_{22} - c_{23})/2\rho, \quad a_5 = c_{33}/\rho \\ \xi_1 &= k_1/\omega, \quad \xi_2 = k_2/\omega, \quad \zeta = k_3/\omega \end{aligned} \quad (4)$$

In the ultrasonic experiment, ξ_1 and ξ_2 are related to the incident angle θ and fiber orientation ϕ (Fig. 1) in the form

$$\xi_1 = \frac{\sin \theta \cos \phi}{\alpha_0}, \quad \xi_2 = \frac{\sin \theta \sin \phi}{\alpha_0} \quad (5)$$

where α_0 is the acoustic wave speed in water (≈ 1.485 mm/ μ s). Then ζ is given by the condition of nontrivial solutions of (3). It can be shown that there are three values of ζ , giving rise to three rays in a given direction:

$$\zeta_k = \sqrt{b_k - \xi_2^2} \quad (k = 1, 2, 3) \quad (6)$$

where

$$\begin{aligned} b_1 &= (\beta/2\alpha) - \sqrt{(\beta/2\alpha)^2 - \gamma/2\alpha} \\ b_2 &= (\beta/2\alpha) + \sqrt{(\beta/2\alpha)^2 - \gamma/2\alpha} \\ b_3 &= \frac{1 - a_5 \xi_1^2}{a_4} \end{aligned} \quad (7)$$

$$\alpha = a_1 a_3, \quad \beta = (a_1 a_2 + a_5^2 - a_3^2) \xi_1^2 - (a_1 + a_2)$$

$$\gamma = (a_2 \xi_1^2 - 1)(a_3 \xi_1^2 - 1)$$

The ray diagram for a plane wave transmitted into a unidirectional composite plate is shown in Fig. 5a. Here R^0 indicates the first 'reflected wave from the top surface of the plate, the rays labeled 1, 2, 3 are associated with' the three transmitted waves inside the plate in a decreasing order of their speeds, the rays labeled 11, 12, . . . and 33 are associated with the waves reflected from the bottom of the plate, and T_1 , T_2 , T_3 indicate the waves transmitted into the fluid through the bottom of the plate. From Snell's law, the velocities V_k , V_l and the angles θ_k , θ_l in the diagram are related through

$$\frac{\sin \theta}{\alpha_0} = \frac{\sin \theta_k}{V_k} = \frac{\sin \theta_l}{V_l} \quad (8)$$

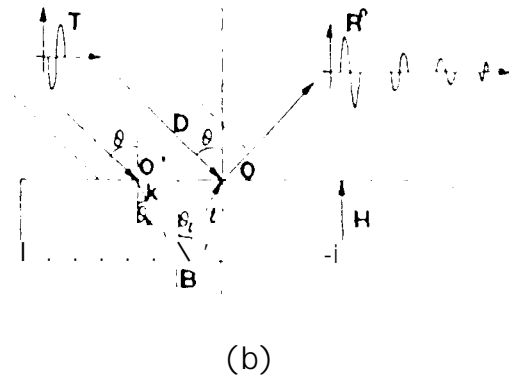
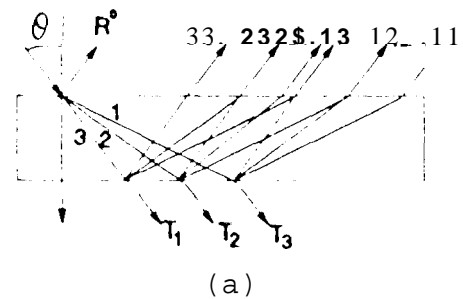


Fig. 5. Ray diagrams of the reflected waves in a unidirectional composite laminate.

Two possible ray paths leading to the same point on the receiver are sketched in Fig. 5b. If we denote the difference in the arrival times between rays along paths DO and O'BO by t_M , then t_M can be expressed as

$$t_M = t_k + t_l - t^D \quad (9)$$

where

$$t_k = \frac{H}{V_k \cos \theta_k}, \quad t_l = \frac{H}{v \cos \theta_l} \quad (10)$$

$$t^D = \frac{H(\tan \theta_k + \tan \theta_l) \sin \theta}{\alpha_0}$$

From (9)-(10), t_M can be expressed as

$$t_M = \frac{H}{V_k \cos \theta_k} + \frac{H}{V_l \cos \theta_l} - \frac{H(\tan \theta_k + \tan \theta_l) \sin \theta}{\alpha_0} \quad (11)$$

$$= \frac{H \cos \theta_k}{V_k} + \frac{H \cos \theta_l}{v} - H(\zeta_k + \zeta_l)$$

It should be noted that equation (11) is valid for homogenous waves only, i.e., when ζ_k, ζ_l are real. In general, there are three possible bulk wave speeds in a composite material, and the recorded time history should contain a reflected pulse from the top surface followed by nine reflected rays from the bottom of the plate and their multiple reflections. However, for a fixed orientation ϕ to the fibers, a certain homogeneous wave will become inhomogeneous or evanescent if the incident angle θ is larger than the critical incident angle. Fig. 6 shows the general feature of this phenomenon, where the wave is propagating along the fiber ($\phi = 0^\circ$) with different incident angles in the range 0° to 9° . It can be seen that for the pulse-echo ($\theta = 0^\circ$) case only the longitudinal waves exist so that the reflected pulses are "11", "111 1" etc. As the incident angle θ increases, the mode converted reflected pulses become more significant. When $\theta \approx 8^\circ$, all of the pulses can be identified clearly. When the incident angle $\theta > \theta_c (\approx 8.4^\circ)$ the pulses with velocity V_1 disappear, and the most prominent pulse is '22'.

Since the wave speed in a composite material is a function of the orientation ϕ , it is possible to have critical values of ϕ for a fixed value of θ . Thus some of the homogeneous waves may become evanescent when the propagation angle ϕ is larger or smaller than a certain critical angle ϕ_c . This is illustrated in Fig. 7, where the reflected pulses near the critical angle for $\theta = 20^\circ$ are presented. It can be seen that the reflected field has a rapid change near the critical angle and some of the pulses disappear when ϕ is smaller than the critical angle.

The Experimental Procedure

With the theory described above, we now describe the experiments and the associated formulas that are needed to determine the five stiffness constants with access from one side of the specimen.

●) Pulse-echo experiment

In this case, $\xi_1 = \xi_2 = 0$, so that from (4)<7)

$$\zeta_1 = \sqrt{\rho/c_{22}}, \quad \zeta_2 = \sqrt{\rho/c_{33}} \quad (12)$$

$$\zeta_3 = \sqrt{2\rho/(c_{22} - c_{23})}$$

and the corresponding eigenvectors for ζ_1, ζ_2 , and ζ_3 are (0, 0, 1), (0, 1, 0) and (1, 0, 0). Since only the longitudinal wave can be transmitted into the fluid from the composite, only the rays associated with ζ_1 exist. Hence the first pulse must be 11, and its arrival time is t_{11} . From (11) and (12),

$$c_{22} = \rho/\zeta_1^2 = 4\rho H^2/t_{11}^2 \quad (13)$$

Thus the pulse-echo experiment provides the constant c_{22} . A simulated result is shown in Fig. 8, where $t_{11} = 16.83 \mu s$. Then c_{22} is found from (13) to be $13.92 \mu s$, in agreement with the value used in the theoretical calculation.

b) Oblique insonification with $\phi = 90^\circ$ and incident angle $\theta > 0^\circ$.

In this case,

$$\xi_1 = 0, \quad \xi_2 = \sin \theta / \alpha_0 \quad (14)$$

$$b_1 = 1/a_1, \quad b_2 = 1/a_3, \quad b_3 = 1/a_4$$

and

$$\zeta_1^2 = -\xi_2^2 + 1/a_1, \quad \zeta_2^2 = \xi_2^2 + 1/a_3 \quad (15)$$

$$\zeta_3^2 = -\xi_2^2 + 1/a_4$$

It should be noted that the eigenvector associated with ζ_2 is (1, 0, 0), indicating that the particle motion is parallel to the fibers, and this transverse wave can not be transmitted into the fluid. Hence, there is no pulse associated with the corresponding ray path, and the arrived pulses should be in the sequence "11", "13", and "33". In this experiment, the direction ϕ is kept fixed and the incident angle is increased from 0° until the pulses "11" and "13" can be identified clearly and t_{11} and t_{13} can be measured. The constants c_{22} and c_{23} can be determined from the formulas,

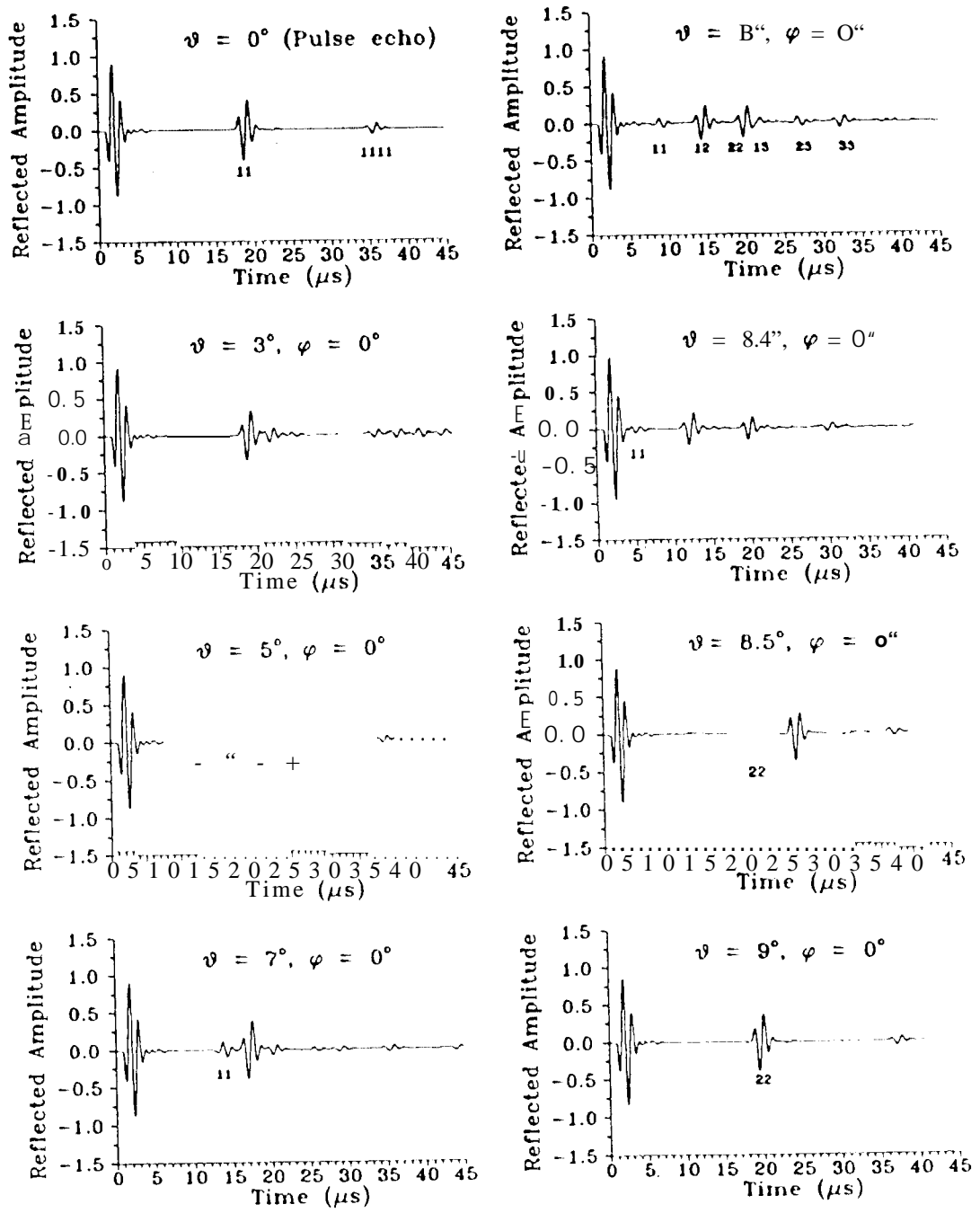


Fig. 6. The reflected signal from a 25 mm thick graphite/epoxy laminate as a function of the incident angle θ for $\phi = 0$.

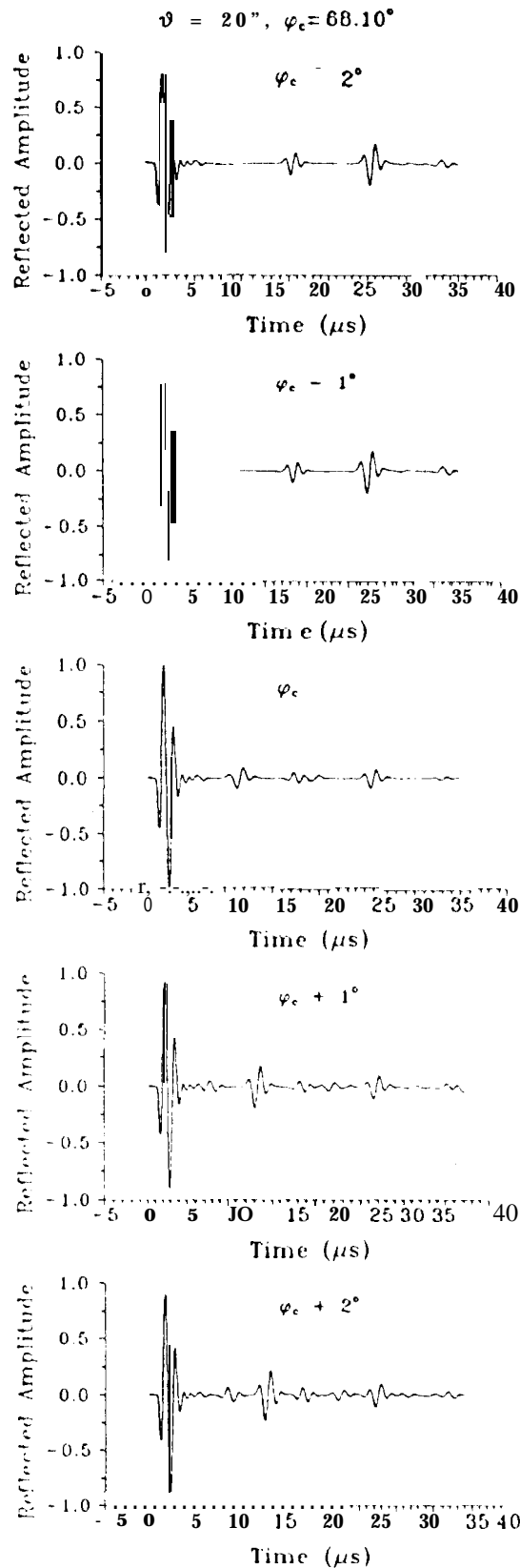


Fig. 7. Reflected signals near critical angle $\varphi_c = 68.1^\circ$ and $\theta = 20^\circ$.

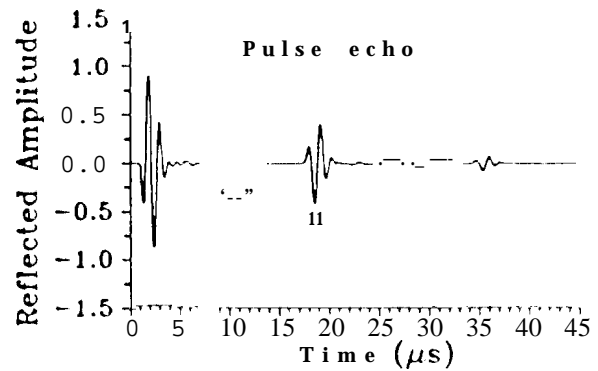


Fig. 8. Reflected signal from a composite laminate in the pulse-echo mode.

$$c_{22} = \frac{\rho}{\left(\frac{t_{11}}{2H}\right)^2 + \frac{\sin^2\theta}{\alpha_0^2}} \quad (16)$$

$$c_{23} = c_{22} = \frac{2\rho}{\left(\frac{t_{13}}{H} - \frac{t_{11}}{2H}\right)^2 + \frac{\sin^2\theta}{\alpha_0^2}}$$

A simulated result for $\theta = 20^\circ$ is shown in Fig. 9, where $t_{11} = 12.28 \mu\text{s}$ and $t_{13} = 21.91 \mu\text{s}$. Then c_{22} and c_{23} can be calculated from (16) as 13.92 GPa and 6.92 GPa, respectively.

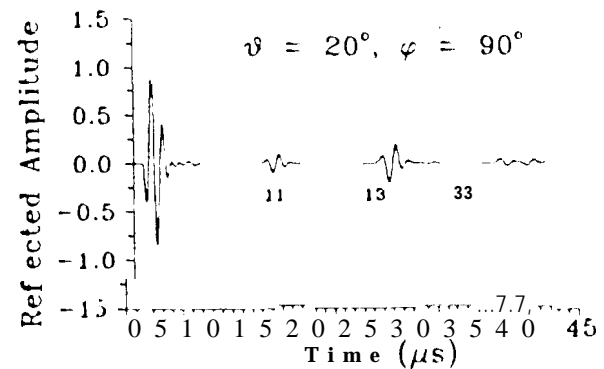


Fig. 9. Reflected signal from a composite laminate for $\theta = 20^\circ$ and $\phi = 90^\circ$.

c) Oblique insonification with ϕ less than the critical angle φ_c .

After c_{22} and c_{23} have been determined, the constant c_{33} can be found as follows. With fixed incident angle θ , adjust ϕ such that the pulses "22" and "23" can be identified clearly. Then from measured

t_{22}, c_{55} can be determined from the formula,

$$c_{55} = \frac{\rho \alpha_0^2}{\sin^2 \theta \cos^2 \phi} \left(1 - \frac{c_{22}}{2} \left[\left(\frac{t_{23}}{H} - \frac{t_{22}}{2H} \right)^2 + \frac{\sin^2 \theta \sin^2 \phi}{\alpha_0^2} \right] \right) \quad (17)$$

A simulated result for $\theta = 20^\circ$ and $\phi = 30^\circ$ is shown in Fig. 10, from which $t_{22} = 22.42 \mu\text{s}$ and $t_{23} = 14.94 \mu\text{s}$. Hence c_{55} can be determined from (17) as 7.08 Gpa.

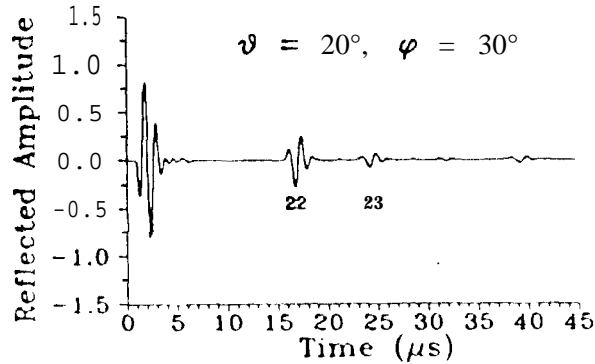


Fig. 10. Reflected signal from a composite laminate for $\theta = 20^\circ$ and $\phi = 30^\circ$.

d) Oblique insonification with $\phi = 0^\circ$

The remaining two unknowns c_{11} and c_{12} , can be determined from this procedure. The time of flight t_{11} and t_{12} can be identified by changing θ from 0° to an angle less than the first critical angle θ_c . Then ζ_1 and ζ_2 can be calculated from (6) and c_{11} and c_{12} can be determined from the equations,

$$c_{11} = \left[- \frac{\alpha_0^2 c_{22} c_{55}}{\rho (c_{55} \sin^2 \theta - \rho \alpha_0^2) \left(\frac{t_{11}}{2H} \right)^2} \left(\frac{t_{12}}{H} - \frac{t_{11}}{2H} \right)^2 + 1 \right] \frac{\rho \alpha_0^2}{\sin^2 \theta} \quad (18)$$

$$c_{12} = \left\{ (c_{11} c_{22} + c_{55}^2) - \frac{\alpha_0^2}{\sin^2 \theta} [\rho (c_{22} + c_{55}) - c_{11} c_{55} \left(\left(\frac{t_{11}}{2H} \right)^2 + \frac{t_{12}}{H} - \frac{t_{11}}{2H} \right)^2] \right\} - c_{55}$$

The simulated results obtained for $\theta = 8^\circ$ is shown in Fig. 11, with $t_{22} = 17.95 \mu\text{s}$, $t_{23} = 25.43 \mu\text{s}$. Then c_{11} and c_{12} are calculated from (18) to be 161.8 GPa and 6.46 GPa, respectively.

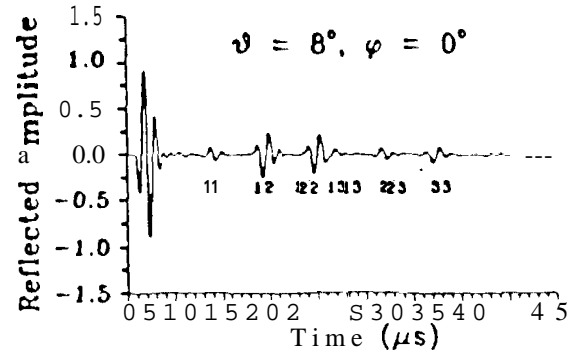


Fig. 11. Reflected signal from a composite laminate for $\theta = 8^\circ$ and $\phi = 0^\circ$.

Since experiment d) is difficult to carry out due to the small incident angle θ , an alternate method is proposed to determine the remaining constant c_{11} and c_{12} . Our calculations have shown that the reflected field changes significantly near the critical angle as can be seen from Fig. 7. Furthermore, the material constants have a strong influence on the reflected signals near the critical angle. To see this, the reflected signals from a 25 mm composite laminate with the original material constants and with the reduced material constants are compared in Figs. 12 and 13. Fig. 12 shows that the arrival times of the pulses "1", "2" and "3" are strongly influenced by the values of c_{11} . The same is true for c_{12} as shown in Fig. 13.

Fig. 14 shows the calculated arrival times of the pulses "1", "2", and "3" with the original material constants and with c_{11} reduced by 20%. Clearly, the arrival times of these pulses are strongly affected by c_{11} near critical angle. We use this critical angle phenomenon to determine the constants c_{11} and c_{12} . Recall that the equation for the bulk wave speed V associated with the constants c_{11} and c_{12} can be written as

$$[(a_1 - a_3) + (a_3 - V^2)/n_2^2] a_2 - a_3^2$$

$$- [(a_3 - V^2)^2 + (a_3 - V^2)(-a_3 + a_1 n_2^2)$$

$$+ a_3(a_1 - a_3)n_1^2 n_2^2]/n_1^2 n_2^2$$

where $n_1 = \cos \phi$, $n_2 = \sin \phi$. The constants a_1, a_2, a_3 can be derived from the known constants c_{22}, c_{23}, c_{55} , and the remaining unknowns a_2 and a_3^2 can be related to c_{11} and c_{12} through eq. (4). In the critical cases $\phi = \phi_c$ and $V = \alpha_0 / \sin \theta$. Hence if we can determine two critical angles from the experiment then the unknowns a_2 and a_3^2 can be calculated from a system of linear equations. In this case, the two

critical angles are $\phi_c = 57.67^\circ$ for $\theta = 15^\circ$, and $\phi_c = 68.10^\circ$ for $\theta = 20^\circ$, so that c_{11} and c_{12} can be calculated as 161.12 and 6.14 GPa., respectively.

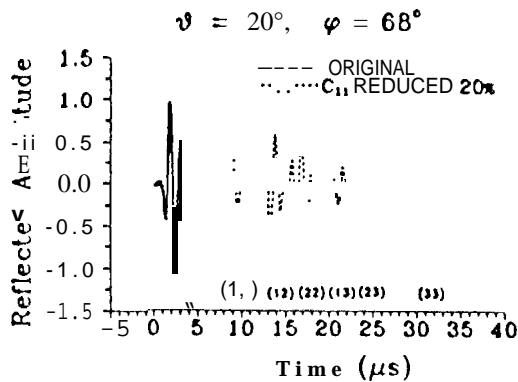


Fig. 12. Influence of the stiffness constant c_{11} on the reflected signal.

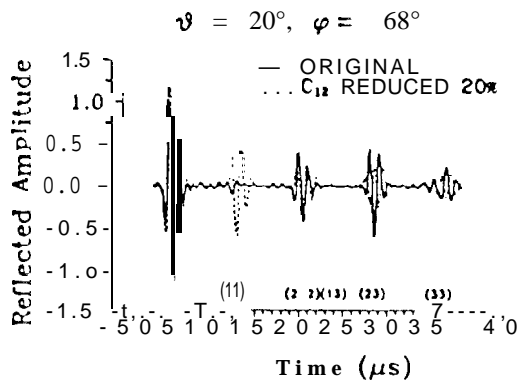


Fig.13. Influence of the stiffness constant c_{12} on the reflected signal.

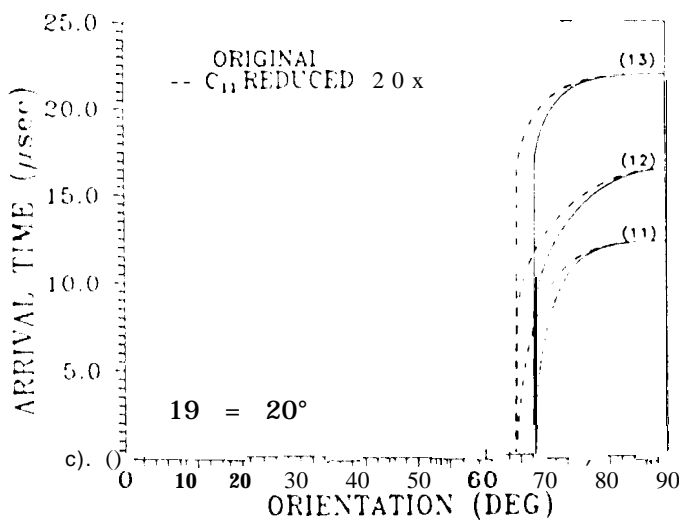


Fig.14. Influence of the stiffness constant c_{11} on the arrival time of the reflected waves.

Error Analysis

An error analysis is carried out in each step of the experiments to determine the accuracy of the proposed technique. as follows:

a) Pulse-echo experiment

$$\delta c_{22} = -(c_{22}/2t_{11})\delta t_{11}$$

If $\delta = \pm 0.02 \mu s$, then $\delta c_{22} = \pm 0.0082 \text{ GPa}$

b) Oblique insonification with $\phi = 90^\circ$ and incident angle $\theta > 0^\circ$.

$$\delta c_{23} = \delta c_{22} + \frac{2(c_{22} - c_{23})}{(\xi_2^2 + \zeta_3^2)}(\xi_2 \delta \xi_2 + \zeta_3 \delta \zeta_3)$$

where $\delta \xi_2 = \cos \theta \delta \theta / \alpha_0$, $\delta \zeta_3 = (\delta t_{13} - \delta t_{33} / 2) / H$

If $\delta \theta = \pm 0.1^\circ$ and $\delta t = 0.02 \mu s$, then $\delta c_{23} = \pm 0.012 \text{ GPa}$.

c) Oblique insonification with ϕ less than the critical angle ϕ_c .

$$\delta c_{35} = \{-2(c_{22} - c_{23})[(\zeta_3^2 + \xi_2^2)]\delta \xi_1 / \xi_1 + (\zeta_3 \delta \zeta_3 + \xi_2 \delta \xi_2)\} + (\delta c_{22} - \delta c_{33})(\zeta_2^2 + \xi_2^2) / \xi_1^2$$

If $\delta \theta = \pm 0.1^\circ$ and $\delta t = 0.02 \mu s$, then $\delta c_{35} = \pm 0.11 \text{ GPa}$. From the above analysis, it can be seen that the constants determined in steps (a), (b) and (c) are very accurate and small errors in the data have small effects on the constants c_{11} and c_{12} .

d) Oblique insonification with $\phi = 0^\circ$

Since the equations for the determination of the constants c_{11} and c_{12} are very complicated, numerical estimates of the errors analysis were carried out and are presented in Fig. 15. It can be seen that the errors in both cases are smaller than 10% if δt_{11} and δt_{12} are less than $0.1 \mu sec$. The errors in c_{11} remain very small for δt_{11} and δt_{12} up to $0.5 \mu sec$. However, the error in c_{12} becomes very large when δt becomes larger. Hence, it is necessary to control the accuracy of the arrival time under $0.1 \mu s$ to accurately evaluate c_{12} .

e) Critical angle experiment:

As in d) it is difficult to obtain analytical estimates of the errors in an explicit form in this case. So we computed the errors by changing measured ϕ and θ by

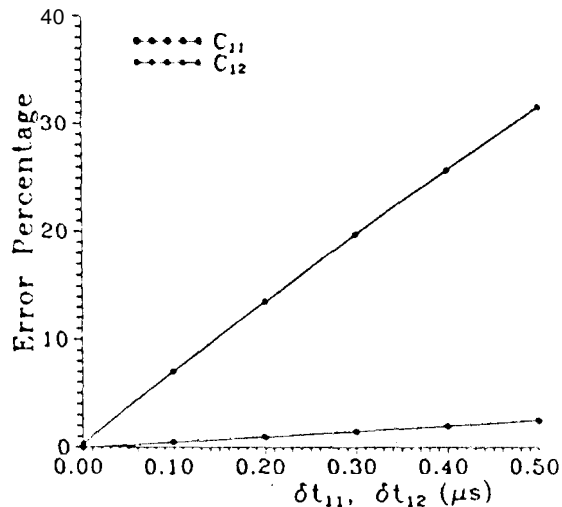


Fig. 15. Errors in c_{11} and c_{12} due to small errors in t_{11} and t_{12} .

small amounts near the critical angles. The results are given in table 1. We can see that the errors in c_{11} and c_{12} induced by measurement errors are small. Hence, this procedure can be an accurate method for practical application.

Table 1. Errors in c_{11} and c_{12} due to errors in ϕ_c and θ .

errors in	calculated		
ϕ_c, θ	c_{11}	c_{12}	
-0.1, -0.1	163.11	5.23	
0.0, 0.0	161.12	6.14	
0.1, 0.1	159.17	6.95	

V. Concluding Remarks

The proposed method appears to be efficient and accurate in characterizing all 5 stiffness constants of a unidirectional fiber-reinforced composite laminate. The error analysis shows that the determined constants are insensitive to small errors in the data. Extension of work will provide a nondestructive procedure that can determine the degree of materials degradation in unidirectional as well as multilayered composite systems.

Acknowledgment

This research was supported by the Mechanics Division of the Office of Naval Research under Contract N00014-90-J-1857 monitored by Dr. Y. D. S. Rajapakse. The part of this study that was carried out at the Jet Propulsion Laboratory (JPL), was performed under a contract with the National Aeronautics and Space Administration (NASA).

References

- Hagemair, D. J., Wendelbo, A. H. and Bar-Cohen, Y., "Aircraft Corrosion and Detection Methods," *Materials Evaluation*, Vol. 43, pp. 426-437, 1985.
- Mat, A. K. and Bar-Cohen, Y., "Nondestructive Characterization of Composite Laminates," *Proceedings of the Mechanics of Composites Review*, Dayton, Ohio, pp. 151-159, 1991.
- Bar-Cohen, Y., "Ultrasonic NDE of Composite - a Review," *Solid Mechanics Research for Quantitative NDE*, J. D. Achenbach and Y. Rajapakse (Eds.), Marinus Nijhoff Publishers, Boston, pp. 197-201, 1987.
- Mal, A. K., Gorman, M. R., and Presser, W. H., "Material Characterization of Composite Laminates Using Low-frequency Plate Wave Dispersion Data," *Review of Progress in Quantitative NDE*, Vol. 11, pp. 1451-1458, 1992.
- Karim, M. R., Mal, A. K., and Bar-Cohen, Y., "Inversion of Leaky Lamb Wave Data by Simplex Algorithm," *J. Acoust. Soc. Am.*, Vol. 88, pp. 482-491, 1990.
- Mal, A. K., Yin, C.-C., and Bar-Cohen, Y., "Analysis of Acoustic Pulses Reflected from the Fiber-Reinforced Composite Laminates," *J. Appl. Mech.* Vol. 59, No. 2, pp. 136-144, 1992.
- Mal, A. K., Bar-Cohen, Y. and Lih, S.-S., "Wave Attenuation in Fiber-Reinforced Composites," *International Symposium on Mechanics and Mechanisms of Material Damping (M'D)*, ASTM STP 1169, pp. 245-261, 1992.